Available online at www.sciencedirect.com
ScienceDirect
Journal of Magnetic Resonance 184 (2007) 85–100
JMR Journal of Magnetic Resonance
www.elsevier.com/locate/jmr

Sensitivity enhancement of NMR spectra of half-integer spin quadrupolar nuclei in solids using hyperbolic secant pulses

Renée Siegel, Thomas T. Nakashima, Roderick E. Wasylishen *

Department of Chemistry, Gunning/Lemieux Chemistry Centre, University of Alberta, Edmonton, Alta., Canada T6G 2G2

Received 17 June 2006; revised 14 September 2006
Available online 13 October 2006

Abstract

The experimental factors influencing the enhancements achievable for the central NMR transition, $m_I = 1/2 \rightarrow m_I = -1/2$, of spin-3/2 and spin-5/2 nuclei in the solid state using hyperbolic secant, HS, pulses for population transfer are investigated. In the case of powder samples spinning at the magic angle, it is found that the spinning frequency, the bandwidth and the frequency offset of the HS pulse play a crucial role in determining the maximum enhancements. Specifically, the bandwidth must be set to the spinning frequency for maximum signal enhancements. The ^{87}Rb NMR enhancement obtained for $RbClO_4$ using HS pulses was relatively insensitive to the magic angle spinning frequency; however, in the case of $Al(acac)_3$, the ^{27}Al enhancement increased with MAS frequency. In order to obtain an adiabatic HS sweep, one should optimize the rf field for a given pulse duration or optimize the pulse duration for a given rf field.

Keywords: Solid-state NMR; Half-integer quadrupolar nuclei; Sensitivity enhancement; Hyperbolic secant pulses

1. Introduction

Roughly two-thirds of all stable NMR-active isotopes are quadrupolar with non-integer spin and of these, approximately 85% have magnetogyric ratios less than ^{13}C [1–4]. Clearly signal-to-noise is a problem in observing NMR spectra for many of these isotopes in solids. Fortunately, the central NMR transition, $m_I = 1/2$ to $m_I = -1/2$, is relatively sharp because it is not perturbed by the first- or third-order quadrupolar interactions [5–7]; thus, it is this transition that has been the focus of most solid-state NMR investigations of these isotopes. The line width of the central transition, CT, is directly proportional to $\nu_Q^2[I(I+1) - 3/4]/\nu_L$, where $\nu_Q = 3C_Q/2I(2I-1)$, ν_L is the Larmor frequency, and C_Q is the nuclear quadrupolar coupling constant which is defined as the product of the nuclear quadrupole moment and the largest principal component of the electric field gradient, EFG, tensor, V_{ZZ}[5–8].

R.V. Pound [6] in 1950, was the first to demonstrate that spin-state populations in a spin-3/2 system could be manipulated by partial continuous wave saturation of the various ^{23}Na NMR transitions in a single crystal of $NaNO_3$. In 1981, Vega and Naor [9] showed that by inversion of the two ^{23}Na NMR satellite transitions in a single crystal of sodium nitrate, the CI could be enhanced by a factor of three in a pulsed NMR experiment. Later, Haase and Conradi [10] and Haase et al. [11] obtained signal enhancements of 5.0 for the central ^{27}Al ($I = 5/2$) NMR transition of a single crystal of Al_2O_3 by sequential adiabatic inversions of the satellite transitions. Similarly, Haase and Conradi [10] realized significant ^{27}Al enhancements for stationary powdered samples of α-Al_2O_3. In 1999, Kentgens and Verhagen [12] obtained CT enhancements of approximately 1.7 for the central ^{23}Na NMR transition of polycrystalline Na_2SO_4 by applying double-frequency sweeps, DFS, to the satellite transitions of $I = 3/2$ spin systems in samples spinning rapidly at the magic angle. In the same paper, the amplitude-modulated DFS pulses were also utilized for the conversion of triple- to single-quantum coherences in multiple-quantum magic angle spinning,

* Corresponding author. Fax: +1 780 492 8231.
E-mail address: Roderick.wasylishen@ualberta.ca (R.E. Wasylishen).

1090-7807/$ - see front matter © 2006 Elsevier Inc. All rights reserved.
doi:10.1016/j.jmr.2006.09.007

MQMAS, experiments. Almost simultaneously, P.K. Madhu et al. [13] also used fast amplitude modulated (FAM) pulses for the same purpose in MQMAS experiments. In 2000, Grandinetti and co-workers [14] introduced the rotor-assisted population transfer, RAPT, experiment to enhance the CT of half-integer quadrupolar nuclei in MAS samples. While the first RAPT experiments employed an $X-\overline{X}$ sequence, a more robust version of RAPT employs frequency switched Gaussian pulses, FSG-RAPT [15]. More recently, Bräuniger et al. [16] used a FAM sequence to enhance the CT of ^{27}Al NMR spectra in both stationary and spinning samples. The DFS and RAPT techniques developed by Kentgens et al. [12,17–21] and by Grandinetti and co-workers [14,15,22–24], respectively, clearly have potential in studying non-integer spin quadrupolar nuclei. We have recently shown that hyperbolic secant, HS, pulses [25–35], which have been used as broad-band inversion pulses in magnetic resonance imaging, MRI, [27,29,34] and in liquid state NMR studies [31], can be used to enhance the sensitivity of the CT for spin-3/2 [36] and spin-5/2 nuclei [37]. As well, we have demonstrated the benefits of HS pulses in MQMAS NMR experiments involving spin-3/2 nuclei in solids [38]. In particular, enhancements for all three Rb sites in $RbNO_3$ realized using HS pulses were superior to previously published methods.

All three enhancement techniques, DFS, RAPT/FAM, and HS, are based on population transfer; that is, the populations of the $m_I = 1/2$ and $m_I = -1/2$ levels are modified either by inverting the populations of adjacent satellite energy levels (e.g., the $m_I = 3/2$ and $m_I = 1/2$ levels as well as the $m_I = -1/2$ and $m_I = -3/2$ levels) or by saturating them [39]. While this is straightforward for NMR studies involving single crystals (*vide infra*), it is much more difficult for investigations involving powder samples where the satellite transitions, STs, may span several MHz.

The purpose of this paper is to provide an evaluation of the experimental parameters of HS pulses that influence the sensitivity enhancement for half-integer quadrupolar nuclei in solids. The HS technique is compared to the DFS and RAPT techniques for several samples. While the focus of this manuscript is on MAS powder samples of spin-3/2 and -5/2 nuclei, the technique is also demonstrated for stationary powder samples.

2. Background theory

2.1. Population Transfer

In a strong applied magnetic field, the equilibrium thermal populations of the nuclear Zeeman energy states can be altered by applying saturation or inversion pulses to one or more NMR transitions. From an energy level diagram applicable to an ensemble of spin-3/2 nuclei [36,39], it is clear that a substantial enhancement in the intensity of the CT can be achieved if the Boltzmann populations are modified [39]. For example, it has been shown [36] that inverting the populations of the $m_I = 3/2$ and $m_I = 1/2$ energy levels prior to selectively exciting the $m_I = 1/2$ to $m_I = -1/2$ transition results in a CT enhancement of up to 2.0. If both the $m_I = 3/2 \rightarrow m_I = 1/2$ and the $m_I = -1/2 \rightarrow m_I = -3/2$ transitions are inverted prior to excitation of the CT, the maximum enhancement due to population transfer is 3.0. It is straight forward to show that an enhancement of 5.0 is possible for an ensemble of spin-5/2 nuclei [37] and, in general, for an ensemble of nuclei of spin I, an enhancement of $2I$ is possible. On the other hand, for a spin-3/2 nucleus, simultaneous saturation of the STs prior to selective excitation of the CT, yields an enhancement of 2.0 or in general, $(I + 1/2)$ [36,37,39].

The theoretical maximum enhancement for the central ^{23}Na NMR transition, 3.0, from a single crystal of $NaNO_3$ can readily be achieved [36]. For powder samples, the maximum enhancements are reduced because the STs are more difficult to manipulate since they are typically spread over frequencies (see Eq. (1), below) of many MHz due to the orientation dependence of the nuclear quadrupolar interaction. In addition, the STs always overlap with the CT [8,40–43] making it difficult to selectively excite the entire ST lineshape without perturbing the CT and *vice versa*. For half-integer quadrupolar nuclei, perturbation of the Zeeman energy levels due to the nuclear quadrupolar interaction to first-order, leads to STs with frequencies given by Eq. (1) [5,8]:

$$\nu_{(m_I \rightarrow m_I - 1)} = (\nu_Q/4)(1 - 2m_I)\{(3\cos^2\theta - 1) + \eta_Q \sin^2\theta \cos 2\varphi\}, \quad (1)$$

where ν_Q has been defined previously. The polar angles θ and φ define the orientation of the principal components of the EFG tensor in the applied magnetic field, $\mathbf{B}_0$ (θ is the angle between V_{ZZ} and $\mathbf{B}_0$), and the quadrupolar asymmetry parameter, η_Q, is equal to $(V_{xx} - V_{yy})/V_{zz}$, where the principal components of the EFG tensor are defined such that: $|V_{zz}| \geqslant |V_{yy}| \geqslant |V_{xx}|$. All NMR transitions including the CT are perturbed to second-order. Expressions for the second-order corrections are given elsewhere [5,8,40–44]; here it is sufficient to note that the magnitudes of the perturbations in frequency units are proportional to C_Q^2/ν_L. As mentioned in Section 1, the main objective of the present study is to examine the utility and experimental parameters necessary for inverting the populations of the states associated with STs in MAS and stationary powder samples using HS pulses. In particular, we will investigate the experimental conditions necessary for achieving maximum enhancements of the CT with minimum lineshape distortion.

2.2. Hyperbolic secant pulses

Hyperbolic secant, HS, pulses, first used in laser spectroscopy in 1969 by McCall and Hahn [25], were used by Silver et al. to provide highly selective, low-power π-pulses for MRI applications [27,28]. The HS pulse inversion pro-

file is independent of the applied rf field, provided that it is above a certain power level [29,31,32,34,35]. The HS pulse is created using both amplitude, $\omega_1(t)$, and phase variation, $\varphi(t)$, which are given by [27,31–35,45,46]:

$$\omega_1(t) = \omega_{1,\max}\operatorname{sech}\left(\beta\left(\frac{2t}{T_p}-1\right)\right), \tag{2}$$

$$\varphi(t) = \left(\frac{\lambda}{\beta}\right)\left(\frac{T_p}{2}\right)\ln\left[\cosh\left(\beta\left(\frac{2t}{T_p}-1\right)\right)\right] + \Delta\omega_0 t, \tag{3}$$

where $\omega_{1,\max}$ is the maximum amplitude of the pulse, T_P is the pulse length, β (=5.3) is a truncation factor which limits the sech function at an amplitude of 1%, λ is equal to one-half of the inversion bandwidth, and $\Delta\omega_0$ is the offset of the HS pulse from the carrier frequency. The phase variation, $\varphi(t)$, generates an effective frequency sweep (i.e., the derivative of the phase), $\Delta\omega(t)$, over the bandwidth centered at a particular offset, $\Delta\omega_0$, given by [46]:

$$\Delta\omega(t) = \lambda\tanh\left(\beta\left(\frac{2t}{T_p}-1\right)\right) + \Delta\omega_0. \tag{4}$$

Population inversion can only occur if the frequency sweep is adiabatic, that is, if the sweep rate is sufficiently slow so that the magnetization vector, $\boldsymbol{M}$, is continuously aligned with $\boldsymbol{B}_{\text{eff}}$. On the other hand, the sweep must be fast enough that longitudinal spin relaxation during the sweep is negligible. Similar requirements also pertain to DFS experiments. For a more detailed discussion on adiabaticity the reader is referred to references [30,31,33,39,47].

Before discussing the requirements for an adiabatic sweep in systems of quadrupolar nuclei [17,47], it is instructive to first discuss a spin-1/2 system. Consider an ensemble of spin-1/2 nuclei described by the following time-dependent Hamiltonian:

$$H(t) = \Delta\omega(t)I_z + \omega_1(t)I_x, \tag{5}$$

where $\Delta\omega(t)$ is the offset of the rf from the exact resonance and $\omega_1(t)$ is the amplitude of the rf field. The effective field, $\omega_{\text{eff}}(t)$, expressed in frequency units, is the vector resultant of $\Delta\omega(t)$ and $\omega_1(t)$. The adiabaticity factor, denoted as A, quantifying the adiabaticity of the pulse, is given by [30,31,47]:

$$A = \frac{\omega_{\text{eff}}(t)}{\frac{\mathrm{d}}{\mathrm{d}t}\alpha(t)} = \frac{[\omega_1^2(t)+\Delta\omega^2(t)]^{3/2}}{\omega_1(t)\frac{\mathrm{d}}{\mathrm{d}t}\Delta\omega(t) - \Delta\omega(t)\frac{\mathrm{d}}{\mathrm{d}t}\omega_1(t)}, \tag{6}$$

where α is the angle between $\mathbf{B}_{\text{eff}}$ and $\mathbf{B}_0$. For the HS pulse the adiabaticity factor is given by [48]:

$$A = \frac{1}{2\beta}\lambda T_p\frac{[\cosh^2(\beta(2t/T_p-1)) + (\omega_{1,\max}/\lambda)^2 - 1]^{3/2}}{(\omega_{1,\max}/\lambda)\cosh^2(\beta(2t/T_p-1))}. \tag{7}$$

Small values of A correspond to rapid changes in the angle α and lead to a sudden passage, i.e., the Hamiltonian varies too rapidly for the magnetization to respond and the state of the system remains unchanged. Under these conditions, the sweep has no effect on the populations of the energy levels. On the other hand, large values of A lead to an adiabatic passage, and inversion of the populations of the energy level occurs. For spin-1/2 nuclei, a passage is generally considered adiabatic when $A \geqslant 1$.

For a spinning powder sample containing quadrupolar nuclei, the expression for the adiabaticity factor is more complicated because the quadrupole frequency, as indicated above, is orientation dependent and due to sample spinning, becomes time dependent. Therefore, A depends on the effective rf field, which is different for each of the possible transitions, the transition quantum number, and the time dependence of the quadrupolar frequency under MAS conditions, $\Omega_{\text{Q}}(\theta,\phi,t)$ [39,47]. For the transition $m_i \leftrightarrow m_{\text{j}}$ under MAS conditions, Schäfer et al. [19] found that at resonance, the adiabaticity factor can be expressed by

$$A_{\text{MAS}}^{i-j} = \frac{\omega_{\Delta m,\text{eff}}^2}{\Delta m\frac{\mathrm{d}}{\mathrm{d}t}[\Omega_{\text{Q}}(\theta,\phi,t) - \Delta\omega(t)]}, \tag{8}$$

where $\omega_{\Delta m,\text{eff}}$ is the effective rf field of the given transition and $\Delta m = m_i - m_j$. Experimentally, the adiabaticity of the HS pulse can be modified by either changing the rf field or the sweep rate, i.e., the bandwidth or the duration of the HS pulse.

3. Experimental

3.1. NMR experiments

All NMR experiments were performed on Bruker Avance NMR spectrometers with wide-bore magnets operating at ^{1}H frequencies of 300 and 500 MHz, corresponding to magnetic field strengths of 7.05 and 11.75 T, respectively. Standard Bruker double-resonance MAS probes accommodating 2.5, 4.0, or 7.0 mm rotors were used. The ^{23}Na and ^{87}Rb NMR experiments were carried out at 7.05 T at frequencies of 79.46 and 98.30 MHz, respectively; the rf field strengths were calibrated and chemical shifts referenced using saturated aqueous solutions of NaCl and RbCl, respectively. The ^{27}Al rf field strengths were determined using powdered samples of α-Al_2O_3 ($B_0 = 7.05$ T, 4 mm rotor) and $Al(acac)_3$ (B_0= 11.75 T, 2.5 mm rotor). The ^{53}Cr NMR measurements were performed at 28.27 MHz ($B_0 = 11.75$ T); a saturated aqueous solution of Cs_2CrO_4 was used to calibrate the rf field strengths and for referencing of the chemical shifts. The ^{55}Mn NMR experiments were performed at 74.27 MHz (7.05 T) and the rf field strength was measured directly on the powder sample of $Mn_2(CO)_{10}$. A powder sample of KI was used to adjust the rf field strength and reference the chemical shift of ^{127}I at a frequency of 100.50 MHz at $B_0 = 11.75$ T. With the exception of NH_4IO_4, all chemicals were commercially available and used without further purification. Ammonium periodate was prepared as described in reference [49].

The HS shapes were created using either the Bruker program ShapeTool which is supplied with the standard Bruker software package or via a Bruker macro-program (au program) using Eqs. (2) and (3). The HS pulse with

two offset values can be generated using two different methods. The first method utilizes cosine amplitude modulation of the HS pulse shape which has the effect of creating sidebands about the carrier frequency in the same manner that the DFS shapes are generated [12]. These shapes are created by executing a macro-program just prior to acquisition of the spectra for ease of spectra optimization. The second method uses two independent rf channels.

3.2. Simulation of NMR spectra using SIMPSON

All the simulations of NMR spectra were carried out using the program SIMPSON [50]. The shape for the HS pulse was created within the SIMPSON input file. Typically the powder averaged spectra were calculated using 10945 crystal orientations and 5 γ angles. The maximum time step over which the Hamiltonian was considered time independent was 0.25 μs, which was also the time step for the HS shape. The SIMPSON simulations for a spin-5/2 system using HS pulses of 4.0 ms took approximately 5 h each to complete running in parallel on a nine processor PC cluster running 2.0 GHz AMD Athion processors.

4. Results and discussion

4.1. Hyperbolic secant inversion pulses applied to spin-3/2 nuclei

4.1.1. ^{87}Rb NMR spectra of polycrystalline $RbClO_4$–a representative spin-3/2 system

We have used ^{87}Rb NMR spectra of polycrystalline $RbClO_4$ to evaluate various sensitivity enhancement techniques under a variety of operating conditions. Rubidium-87 has a spin of 3/2, a natural abundance of 27.8%, and a relatively large magnetogyric ratio ($\Xi =$ 32.72 MHz) which together yield an overall receptivity of 290 relative to ^{13}C. For solid $RbClO_4$, the ^{87}Rb nuclear quadrupolar coupling constant, C_Q, and quadrupolar asymmetry parameter, η_Q, have been studied as a function of temperature [51]. At 20 °C, $C_Q = 3.29$ MHz and $\eta_Q = 0.24$ [52] which leads to a powder ^{87}Rb NMR line shape that falls over a frequency range of C_Q. The breadth of the central ^{87}Rb NMR transition under rapid MAS is $3C_Q^2(6+\eta_Q^2)/2016\nu_L$ or 6.3 kHz at 7.05 T ($\nu_L =$ 98.30 MHz). In a recent letter, we demonstrated that by using HS pulses to invert the populations of the ^{87}Rb NMR STs, an enhancement of 2.7 could be obtained for the CT in a powder sample of $RbClO_4$ under conditions of MAS [36]. This enhancement, achieved using an HS bandwidth of 10 kHz on a sample spinning at 10 kHz, was superior to other methods of population transfer previously used, namely, DFS and RAPT, which gave enhancements of 2.0 and 1.8, respectively. In Fig. 1, the enhancements obtained using DFS, RAPT, and HS techniques are compared using a Hahn-echo [53]. In each case, a Hahn-echo was used to acquire the ^{87}Rb NMR spectrum. Analogous results were also obtained using the quadrupolar Carr-Purcell Meiboom-Gill, QCPMG, experiment [36,52,54–57]. Only a small distortion on the CT of the low-frequency shoulder was noted in the line shape using the HS pulse (see in Fig. 1d). This distortion could be removed by setting one of the HS frequency offsets closer to the center band (from +620 to +310 kHz as illustrated in Fig. 1e). However, the small line shape distortion does not affect the accuracy in determining C_Q or η_Q values. This distortion in the enhanced CT spectrum can be easily explained by examining the contribution made by various crystallites to the CT spectrum under conditions of MAS. For simplicity, we consider a powder sample with an axially-symmetric EFG (i.e., $\eta_Q = 0.0$). The angle, γ, is defined as the angle between V_{ZZ} and the rotor axis (see Fig. 2a). The CT "resonance frequency" as a function of γ is illustrated in Fig. 2b. In order to obtain the CT lineshape shown in Fig. 2c, one must, of course, perform the appropriate powder average (e.g., see Section 2.6, pp. 40–50 of Ref. [58], Section 3.9, pp 102–115 of Ref. [59], and Section 7.3, pp. 170–80 of Ref. [60]). The CT lineshape is independent of spin quantum number; however, the line width of the CT does depend upon I. Several angles in Fig. 2 are noteworthy. Those nuclei within crystallites whose V_{ZZ} are inclined at an angle of approximately 22° and 90° contribute to the right-hand "horn" and those at about 49° comprise the left-hand "horn". Nuclei within crystallites with V_{ZZ} parallel with the magic angle ($\gamma = 0$) contribute to the right-hand shoulder shown in Fig. 1e and Fig. 2c; the position where the distortion occurs. It is therefore

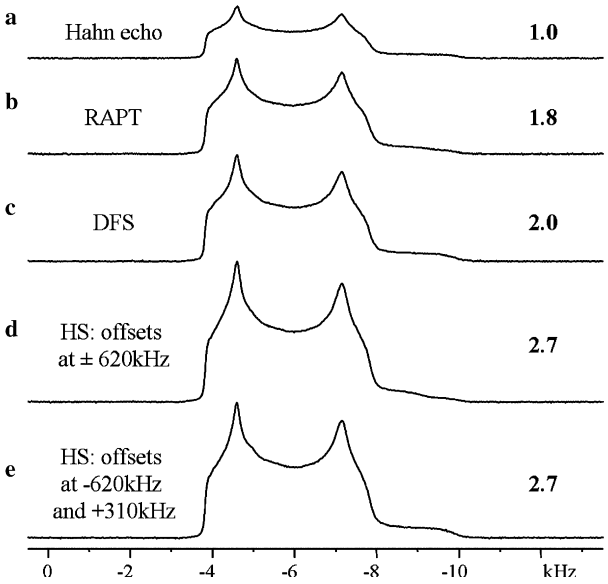

Fig. 1. Comparison of the ^{87}Rb NMR signal intensity of a powder sample of $RbClO_4$, magic angle spinning at 10 kHz, obtained with, (a) Hahn-echo ($\gamma B_1/2\pi = 12.5$ kHz, $\tau_1 = 100$ μs, $\tau_2 = 80$ μs) and with (b) RAPT ($\gamma B_1/2\pi = 100$ kHz, $p_{RAPT} = 0.55$ μs, width of RAPT pulses, $d_{RAPT} = 0.2$ μs, delay between RAPT pulses, $n = 60$, number of RAPT cycles), (c) DFS ($\gamma B_1/2\pi = 27$ kHz, $\nu_{start} = \pm 1750$ kHz, $\nu_{end} = \pm 300$ kHz, $\tau = 5.0$ ms, duration of DFS sweep), and (d and e) HS ($\gamma B_1/2\pi = 27$ kHz, $T_P = 2.3$ ms) enhancement techniques. Numbers to the extreme right of spectra indicate the enhancement relative to the standard Hahn-echo experiment.

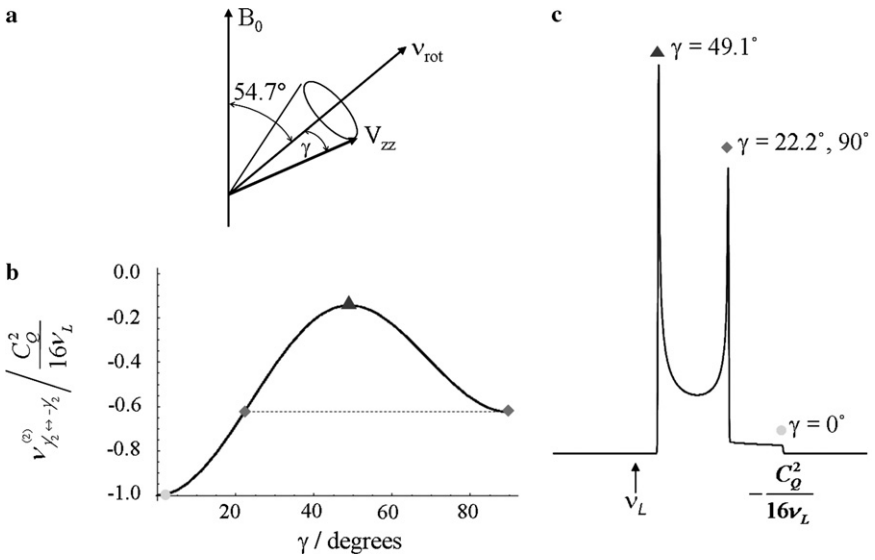

Fig. 2. The orientation (a), defined by the angle γ, of the principal component of the EFG tensor, V_{ZZ}, relative to the spinning axis. The frequency (b), $\nu^{(2)}$, in units of $C_Q^2/(16\nu_L)$, for γ angles from 0 to 90°, from the Larmor precession frequency, ν_L, and (c) their contribution to the powder pattern (several angles indicated). Simulations are for $I = 3/2$ and $\eta_Q = 0.0$.

these nuclei within crystallite orientations with V_{ZZ} at and close to the magic angle that create this distortion in the shoulder because their resonant frequencies are not swept through the HS pulses.

4.1.1.1. Effect of HS frequency offset on enhancement. The maximum signal enhancement achievable for the CT depends upon how effectively the populations of the STs are inverted without perturbing the CT. Thus, the frequency offsets of the HS pulses are expected to play an important role in determining the enhancement factors. Although the ST frequencies for an MAS sample cover the entire frequency range of the complete powder pattern, there are some crystal orientations that are more probable at any given time. A plot of the relative enhancement obtained from the ^{87}Rb NMR CT of a powder sample of $RbClO_4$ spinning at 10 kHz as a function of offset is shown in Fig. 3. The two HS offsets were varied simultaneously from $\pm$ 50 kHz to $\pm$ 1.8 MHz in steps of 10 kHz, a frequency range that covers the entire powder pattern. An

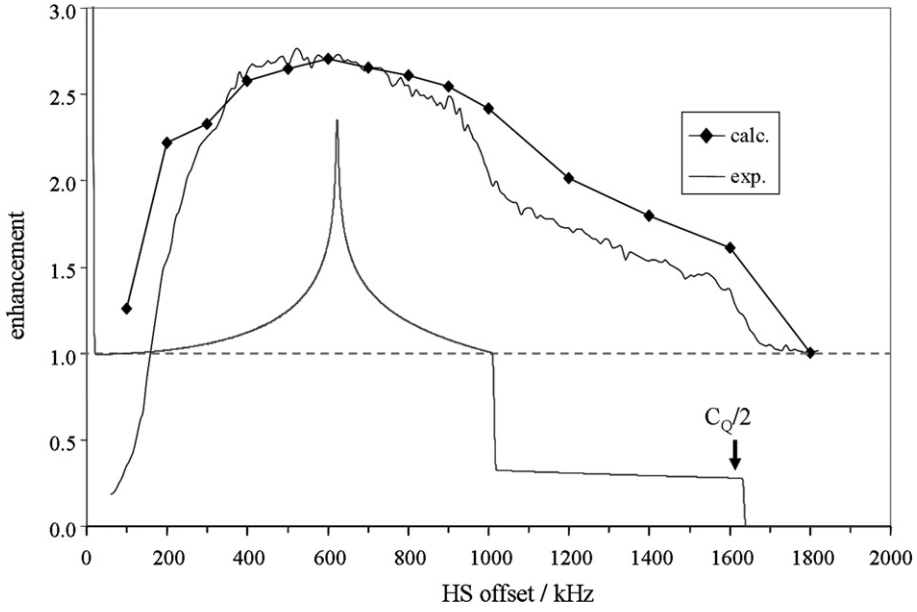

Fig. 3. Comparison of the experimental and simulated values computed by SIMPSON [50] of the relative enhancement of the central transition of ^{87}Rb NMR spectra obtained from a powder sample of $RbClO_4$ spinning at 10 kHz. Experimental data were obtained with a Hahn-echo sequence ($\gamma B_1/2\pi = 25$ kHz, $\tau_1 = \tau_2 = 100$ μs) as a function of the HS offsets, generated with cosine amplitude modulation, placed symmetrically about the carrier. $B_0 = 7.05$ T. Shown in the inset is one half of the theoretically calculated powder pattern for a stationary sample.

HS bandwidth, bw, of 10 kHz, a pulse length of 10.0 ms, and an rf field of 50 kHz (~25 kHz for each offset) were used for the HS pulses. As expected, from the theoretical ^{87}Rb NMR powder pattern of a stationary sample, also shown in Fig. 3, the maximum enhancement occurs at an offset value of approximately 600 kHz which corresponds to the positions of the "horns" of the stationary powder pattern for this sample. A broad maximum in the enhancement of 2.7 is achieved for offsets between $\pm$ 400 and $\pm$ 950 kHz followed by shoulders in the enhancement profile occurring at $\pm$ 1000 and $\pm$ 1600 kHz. These experimental shoulders correspond to the inflection points as predicted from the calculated powder pattern spectrum (see Fig. 3). The first shoulder at 1000 kHz, corresponds to the position where the overlap of the $3/2 \leftrightarrow 1/2$ with the $-1/2 \leftrightarrow -3/2$ transitions ceases which leads to a loss of signal as a result of the decrease in the number of available crystallites with nuclei whose ST are at these frequencies. At this HS offset frequency, distortions in the CT also begin to appear (see Fig. 4) because at this particular frequency, nuclei in some crystallite orientations (those with $\gamma \sim 22°$ and 90°) do not contribute to the spinning side band, ssb, pattern generated by the ST, thus creating the distortions in the CT observed for these HS offsets near 1300 kHz (Fig. 4). A more detailed description of the relationship between distortions in the ssb pattern effecting the CT enhancement will be presented below (Section 4.1.1.3). The second shoulder, at $\pm$ 1600 kHz, is close to $C_Q/2$, where the powder pattern ceases as there are no crystallites with nuclei having ST frequencies outside this range. Thus with an offset value of 1700 kHz ($>C_Q/2$), there no longer is an enhancement of the signal. Similarly, offsets near the carrier lead to perturbation of the CT and enhancements less than 1.0. This overall experimental behavior is reproduced by the simulations performed using SIMPSON [50] (HS pulse of 4.0 ms, rf power of 50 kHz and a bw of 10 kHz) as shown in Fig. 3. The calculated enhancements are slightly higher than those determined experimentally for offsets spanning a frequency range of 1000–1600 kHz and may be the consequence of the quality factor, Q, of the probe coil which limits the effective rf power available at these larger offset frequencies. Using the cosine modulation wave shape, a small modulation of the enhancement with the HS offset as a function of the spinning frequency was observed. Maximum enhancements were achieved at offsets that were multiples of the spinning frequency. On the other hand, using the two channel configuration, this modulation was absent. One should also note that using a single frequency HS pulse on either side of the CT provides enhancements near those obtainable using the HS pulses applied symmetrically about the CT.

In conclusion, an enhancement of the CT greater than 2.0, the usual limit using DFS and RAPT/FAM, can be obtained for a relatively large range of offset frequencies (from approximately 250 to 1000 kHz, experimentally), indicating that the HS pulses are capable of providing larger enhancements than DFS or RAPT for nuclei having a relatively large range of C_Q values.

4.1.1.2. Effect of MAS frequency on the enhancement. The spinning frequency had very little effect on the enhancement within the range of spinning frequencies accessible in our laboratory. Enhancements of approximately 2.7 were obtained for spectra acquired with sample spinning rates of 7.5, 10, 12.5, and 14 kHz, provided that the bw is set to the spinning frequency (as discussed below).

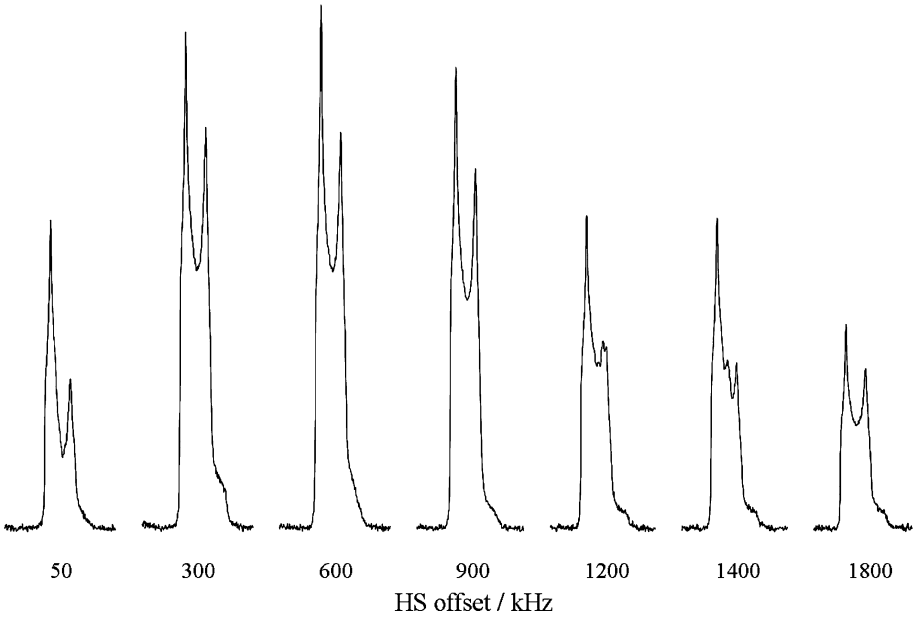

Fig. 4. The ^{87}Rb NMR CT spectrum of a powder sample of $RbClO_4$ spinning at 10 kHz obtained at various values of the HS offset (shown below each spectrum) with a bw of 10 kHz. $B_0 = 7.05$ T.

4.1.1.3. Effect of HS bandwidth on enhancement. Another important parameter determining the enhancement of the CT is the bw of the HS pulses, which ultimately determines the inversion profile width of the HS pulse (see, for example, reference [39]). The enhancements obtained for the CT of the ^{87}Rb NMR signal from a powder sample of $RbClO_4$ were measured as a function of the bw; the results are shown in Fig. 5. The bw was varied from 1 to 100 kHz in steps of 1 kHz for different spinning rates and at two rf field strengths when spinning at 10 kHz. The HS offset was set near ±620 kHz and the pulse width, T_P, set to 10.0 ms. The largest enhancement, 2.7, occurs when the HS bandwidth is set to the spinning frequency. A minimum enhancement of approximately 1.5 is obtained when the bw is set at $2\nu_r$, while a secondary maximum enhancement of 2.3 occurs at $3\nu_r$. The oscillatory behavior of the enhancement with bw decays when the bw is set at approximately 50 kHz or greater. At these HS bandwidths, the enhancement factor is approximately 2.0. As shown in Fig. 5, this experimental trend is reproduced by SIMPSON [50] for $\nu_r = 10.0$ kHz.

Occasionally distortions in the CT occur depending upon the bw and/or the offset of the HS pulse. Before we examine lineshape distortions of the CT, it is instructive to discuss the calculated spectrum one would observe for ^{87}Rb in $RbClO_4$ if the sample were spinning infinitely fast (see Fig. 6). Two peaks would be observed: one for the STs, which is labeled ST1, and one for the CT [61]. The frequencies and the relative linewidths of the ST1 compared to the CT may be calculated using the equations derived by Samoson [62], which are given by, respectively,

$$\mathrm{ST1} - \mathrm{CT} = (3/40)\left[C_Q^2/\nu_L\right]\left[1 + \eta_Q^2/3\right] \tag{9}$$

and

$$\Delta(\mathrm{ST1})/\Delta(\mathrm{CT}) = -0.8889 \tag{10}$$

for a spin-3/2 nucleus. The negative value in Eq. (10) simply indicates a reversal in lineshape between the CT and ST1. In practice, spinning frequencies are generally much less than the value of C_Q, thus ssbs result from ST1 which span C_Q. Spinning side bands from the CT are usually negligible unless the magnetic shielding experienced by the quadrupolar nucleus is highly anisotropic or C_Q is large.

If the HS pulse is positioned to "invert" only part of a ssb generated from the satellite transition, then distortions in the CT occur as mentioned above. For example, if the HS pulse is positioned to only invert the high-frequency component of a particular ssb, then the low-frequency component of the CT is enhanced, as expected from Eq. (10), and vice versa. This effect is illustrated in Fig. 7 where the experimental ^{87}Rb NMR spectra were obtained using the Hahn-echo experiment on a powder sample of $RbClO_4$ spinning at 10.0 kHz with HS offsets ranging from 593 to 602 kHz, incremented in 1 kHz steps, and with a HS bandwidth of 5 kHz. The separation between the CT and ST1 is calculated to be 8.5 kHz, based on the ^{87}Rb C_Q and η_Q values for $RbClO_4$, (Eq. (9)). Thus the 59th order ssb for the ST1 is at a frequency of 598.5 kHz from the carrier frequency which is placed approximately at the center of the CT. It is clear from Fig. 7 that maximum enhancement occurs when the HS pulse is centered on the 59th ssb. The distortions in the CT are also evident in the spectra shown in Fig. 7 and are reproduced by SIMPSON calculations. It is only necessary to invert one ssb generated from the ST1 to obtain maximum enhancement. This observation is consistent with results involving selective pulses on

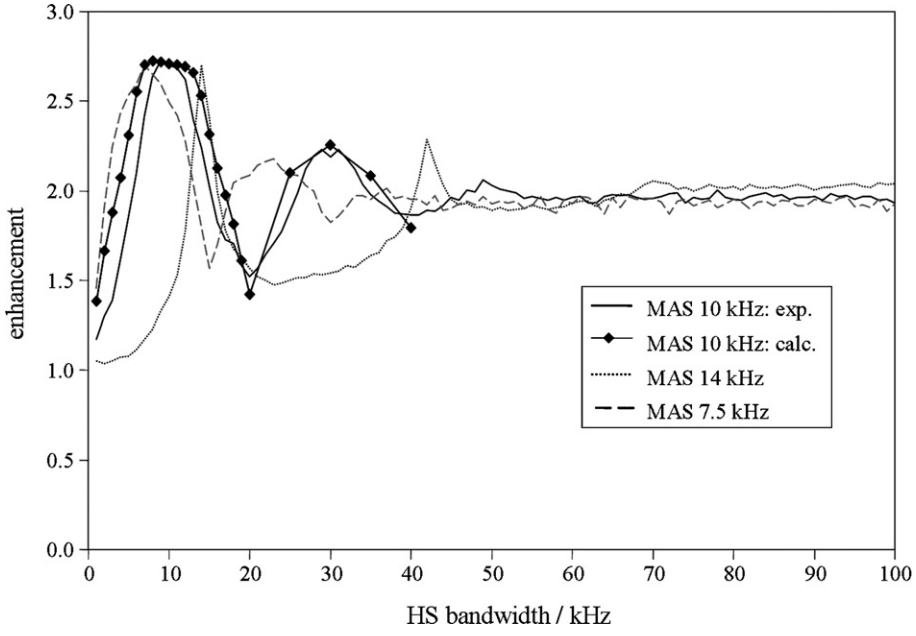

Fig. 5. Relative enhancement of the ^{87}Rb NMR spectra obtained from a powder sample of $RbClO_4$ at several spinning frequencies as a function of the bandwidth of the HS pulse, and comparison of the experimental versus the simulated values obtained with SIMPSON [50] at MAS 10 kHz. $B_0 = 7.05$ T.

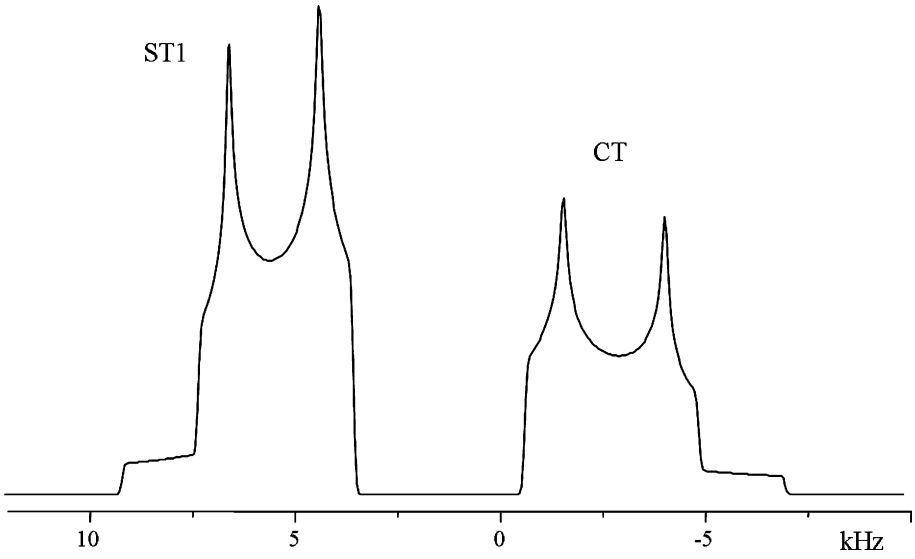

Fig. 6. Calculated NMR spectrum for ^{87}Rb of $RbClO_4$ at 7.05 T at infinite spinning frequency showing both the CT and the ST1.

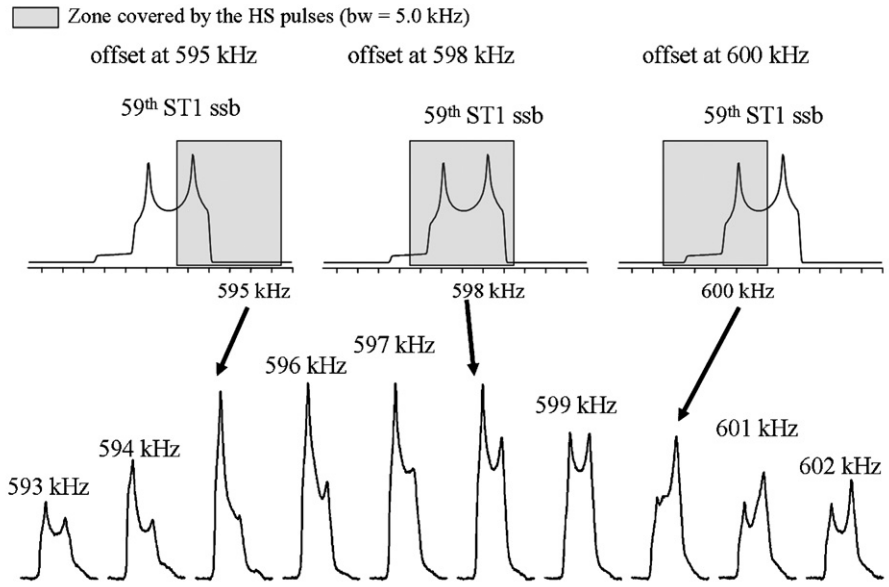

Fig. 7. Central transition ^{87}Rb NMR spectra of $RbClO_4$ (bottom) as a function of HS offset (in kHz above spectra) with a bw of 5 kHz. $B_0 = 7.05$ T. Position of the HS pulse on the 59th ssb generated from ST1 is simulated on top with arrows pointing to the effect on the CT spectrum. Shaded areas represents frequency over which HS pulse is effective.

spin-1/2 nuclei reported by P. Caravatti, G. Bodenhausen, and R.R. Ernst in 1983 [63].

As seen in Fig. 5, the maximum enhancement in the CT is obtained when the bw is equal to the spinning frequency, which is consistent with our observation that only one entire ssb need be inverted with the HS pulse. The minimum in the enhancement observed when the bw is twice the spinning frequency may indicate that some of the nuclei in certain crystal orientations experience an effective 2π or 360° pulse leading to a lower overall enhancement of the CT. As the bw is further increased to three times the spinning speed, perhaps some of the nuclei in a given crystalline orientation experience an effective π-pulse ($3 \times 180°$) leading to another secondary maximum and so forth until the bw effects many ssbs representing a series of 180° pulses which would have the effect of saturation of the satellite transitions, thus leading to an enhancement of 2.0. While this explanation is clearly overly simplistic, it does reproduce the experimental trends.

4.1.1.4. Effect of HS rf-field and pulse duration on enhancement. The last parameters investigated are the HS rf field strength and the pulse length, T_P. Using again the ^{87}Rb NMR CT of $RbClO_4$ spinning at 10.0 kHz, the relative enhancement obtained with HS pulses just prior to a Hahn-echo experiment for two different rf power levels

and at two spinning frequencies were plotted as a function of the pulse width, T_P, of the HS pulses. The experimental results are shown in Fig. 8 together with those calculated using SIMPSON. As the pulse width of the HS pulses (using a $\gamma B_1/2\pi$ of 50 kHz) is increased from 250 μs to 14 ms for the sample spinning at 10 or 14 kHz, there is an initial exponential increase in the intensity which asymptotically approaches a value of 2.8. As seen in Fig. 8, the maximum enhancement is reached much slower with lower rf power. Since the inversion profile of the HS pulse is independent of the applied rf field provided that it is above a certain minimum power level, changing the rf field above that minimum power value only affects the adiabaticity factor, A; however, it was found that for a given pulse duration, too high a rf field decreases the intensity of the CT. Too little power also diminishes the enhancement. To a first approximation, the adiabaticity factor, $A \propto (\omega_1^2$ and $T_P)$ (see Eq. (7)); thus an increase of the rf amplitude, the pulse length, or both increases A for the STs and increases the enhancement for the CT. However, if the rf field is too strong, the potential exists to form double quantum transitions [47], see Eq. (8), which will diminish the CT enhancement. The results obtained for the two different spinning rates (10 and 14 kHz), are almost identical. It thus appears that the increase of the spinning frequency is mostly compensated by the increase in the bandwidth (i.e., bw $= \nu_r$). Even though our experimental results indicate that it is only necessary to set up the HS pulse to effectively invert one spinning side band, it is interesting to note that when $T_P = 4$ ms and $\nu_r = 10$ kHz, the sample makes 40 complete revolutions during the pulse.

In conclusion, for our spin-3/2 test sample, optimum enhancement of the CT NMR signal occurs when the HS offset frequency is set close to the "horns" of the stationary powder pattern with a broad maximum around this value and when the bw of the HS pulse is equal to the spinning frequency. The pulse width of the HS pulse needs to be chosen properly to obtain an adiabatic HS pulse but is not too critical beyond a given value, provided that the rf field is not too strong. The rf field and/or the sweep duration should be optimized on a standard sample and used for other similar classes of compounds, i.e., those with similar nuclear quadrupolar coupling constants.

4.1.2. Further examples of spin-3/2 systems

Sensitivity enhancements obtainable with HS are demonstrated for two other spin-3/2 nuclei, ^{23}Na and ^{53}Cr. As stated before, the maximum enhancements using HS were obtained by setting the HS pulse bw at ν_r, the offsets at or near the horns of the powder pattern and by optimizing the pulse width for a given rf field. The ^{23}Na NMR spectra for a powder sample of Na_2MoO_4, $C_Q = 2.59$ MHz, and $\eta_Q = 0.0$ [64], $\nu_r = 10$ kHz showed an enhancement of 2.5 using the HS pulse versus about 1.9 using either DFS or RAPT. An enhancement close to 2.4 can be obtained by applying one HS pulse at one offset. The smaller enhancement obtained for ^{23}Na compared to that obtained for ^{87}Rb may be due to the stronger homonuclear dipolar coupling occurring for ^{23}Na (natural abundance of 100% compared to 27.8% for ^{87}Rb). Such coupling may lead to transitions between neighboring ^{23}Na nuclei which reduces the efficiency of the selective population inversion [14]. The ^{53}Cr NMR spectra for an MAS powder sample of Cs_2CrO_4, $C_Q = 1.23$ MHz and $\eta_Q = 0.23$ [65], show an enhancement of 2.6 using HS versus about 1.8 for both DFS and RAPT.

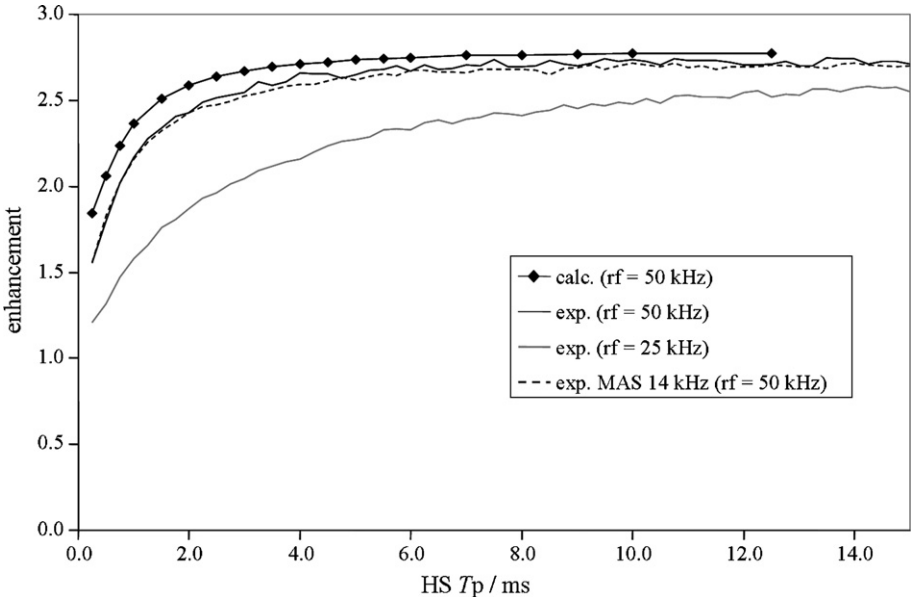

Fig. 8. Comparison of the experimental versus the simulated values by SIMPSON [50] of the relative enhancement of the ^{87}Rb NMR spectra obtained from a powder sample of $RbClO_4$ with MAS at 10 kHz (bw = 10 kHz) as a function of the pulse width, T_P, of the HS pulse. $B_0 = 7.05$ T. Experimental results also shown at two different rf fields with the bw constant at 14 kHz while spinning at 14 kHz. The lower curve corresponds to an rf field of 25 kHz.

Enhancements obtained for other compounds containing spin-3/2 nuclei are summarized in Table 1. The enhancements using HS are quite similar, varying from 2.4 to 2.7 for nuclei having a range of C_Q values (1.2–3.3 MHz) and asymmetry values (0.0–0.74). The smallest enhancement of 1.6 was obtained for ^{23}Na in $NaNO_3$ probably because of the small value of C_Q which prevents the optimization of the HS offset without perturbing the CT.

Previously only DFS was used to enhance the CT of stationary powdered samples; however, since the effective frequency of an HS pulse is also swept, it should be able to enhance the signal from stationary powder samples of half-integer quadrupolar nuclei. The application of HS pulses produced enhancements of 2.6 versus 2.5 using DFS from stationary samples using ^{87}Rb NMR of $RbClO_4$ as shown in Fig. 9. The HS method gives a slightly higher enhancement presumably because of the higher frequency selectivity of the HS pulse, i.e., the sweep may be terminated closer to the CT with HS than with DFS. This problem with the DFS experiment could be attenuated by ensuring that the DFS stops at a frequency with null amplitude, for example, by applying a cosine-squared shape at the end of the DFS shape [19]. To obtain maximum enhancements on stationary samples, both techniques must use frequency sweeps (ν_{start} and ν_{end}, and bw, for DFS and HS, respectively) that cover most of the ST pattern and both sides of the CT must be irradiated.

Table 1
CT enhancements obtained using HS inversion pulses for spin-3/2 and -5/2 nuclei in various samples spinning at the magic angle

	Compound	C_Q/MHz	η_Q	Enhancement[a]	Ref.[b]
$I = 3/2$	$RbClO_4$ (^{87}Rb)	3.3	0.24	2.7	[52]
	Na_2SO_4 (^{23}Na)	2.6	0.58	2.6	[70]
	Na_2MoO_4 (^{23}Na)	2.6	0.0	2.5	[64]
	$Na_2C_2O_4$ (^{23}Na)	2.5	0.74	2.7	[67]
	Cs_2CrO_4 (^{53}Cr)	1.2	0.24	2.4	[65]
	$NaNO_3$ (^{23}Na)	0.3	0.0	1.6	[67]
$I = 5/2$	$Al(acac)_3$ (^{27}Al)	3.0	0.15	4.1	[66]
	Al_2O_3 (^{27}Al)	2.4	0.0	1.8	[71]
	$Mn_2(CO)_{10}$ (^{55}Mn)	3.0	0.5	3.1	[68]
	NH_4IO_4 (^{127}I)	10.0	0.0	2.8	[49]
	Kaolinite (^{27}Al)	3.1	0.95	1.9	[72,73]

[a] Current report.
[b] Quadrupolar parameters obtained from these references.

4.2. Hyperbolic secant inversion pulses applied to spin-5/2 nuclei

4.2.1. ^{27}Al NMR spectra of polycrystalline $Al(acac)_3$–a representative spin-5/2 system

Investigations on the application of HS pulses to enhance the CT NMR signal from half-integer quadrupolar nuclei of higher spin are now well underway. For spin-5/2 nuclei we chose the ^{27}Al NMR response from $Al(acac)_3$ as our standard because ^{27}Al has a large receptivity to NMR detection. For $Al(acac)_3$, the ^{27}Al quadrupolar coupling constant, C_Q, is 3.03 MHz and the asymmetry parameter, η_Q, is 0.15 [66]. The NMR powder pattern spans a frequency range of approximately 1820 kHz with maximum satellite transition intensities occurring at approximately ±400 and ±200 kHz from the central transition. A maximum signal enhancement of 2.8 occurs using DFS while an enhancement of 4.1 is obtained using the HS

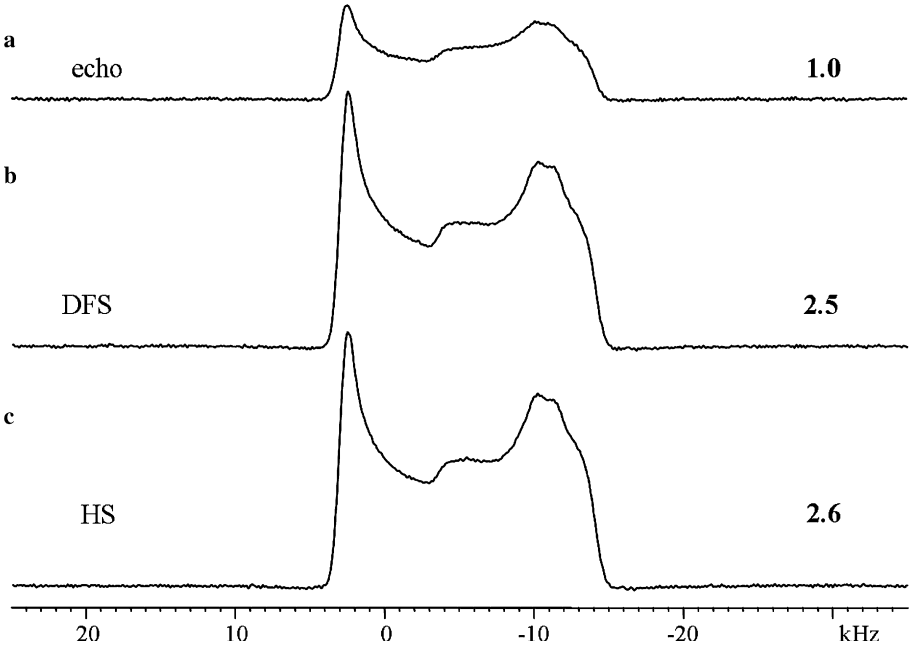

Fig. 9. Comparison of the ^{87}Rb NMR signal intensity of a stationary powder sample of $RbClO_4$ obtained with a Hahn-echo experiment ($\gamma B_1/2\pi = 25.0$ kHz) with (a) no enhancement and with (b) DFS ($\gamma B_1/2\pi = 21$ kHz, $\nu_{start} = \pm 100$ kHz, $\nu_{end} = \pm 1750$ kHz, $\tau = 15.0$ ms) and (c) HS ($\gamma B_1/2\pi = 41$ kHz, bandwidth = 1750 kHz, offsets = ±950 kHz, $T_P = 15.0$ ms) enhancement techniques. $B_0 = 7.05$ T.

pulses with offsets at ±240 kHz relative to the central transition, which is more than 80% of the theoretical maximum enhancement, 5.0, and is the best signal enhancement achieved thus far for a spin-5/2 nucleus from a spinning powder sample [37]. One interesting feature in the spin-5/2 NMR spectra of rapidly spinning powder samples is the observation of the $\pm 3/2 \leftrightarrow \pm 1/2$ satellite transition to high-frequency of the central transition. As expected, the relative intensity of the satellite transition decreased as the intensity of the CT increased.

4.2.1.1. Effect of HS frequency offset on enhancement. The choice of the HS offset frequency for maximum signal enhancement is more difficult to predict for the spin-5/2 nucleus in a powder sample because of the presence of the two overlapping STs ($\pm 3/2 \leftrightarrow \pm 1/2$, ST1, and $\pm 5/2 \leftrightarrow \pm 3/2$, ST2). For a single crystal sample the choice of the inversion pulse frequencies is straightforward and an enhancement of 4.8 was obtained for the central ^{27}Al NMR transition of a single crystal of α-Al_2O_3 [37]. One might predict that to obtain the highest enhancement from a spin-5/2 nucleus, one should simply set the bandwidth of the HS pulse equal to the spinning frequency, and apply HS inversion pulses first at the offsets corresponding to the maximum intensities for the ST2, followed by inversion pulses at offsets corresponding to the maximum intensities for ST1. This approach, however, requires a considerable knowledge of the quadrupolar parameters of the nucleus under investigation and largely defeats the advantages of this sensitivity enhancement technique. Moreover, because the transitions overlap, it is almost impossible to apply an adiabatic sweep on ST1 without affecting ST2. In an MAS powder sample, however, ssbs from both ST1 and ST2 can be separated provided that the spinning frequency is high enough. Thus, we simply use HS pulses with offsets positioned on the maximum distribution of crystallites as found for spin-3/2 nuclei. By setting the HS bw equal to the spinning frequency, we ensure inverting ssbs from both ST2 and ST1. Unlike a spin-3/2 system, the sweep direction of the HS pulse is important. Experimental enhancements of about 3.2 on the ^{27}Al NMR CT of $Al(acac)_3$ were obtained spinning at 10 kHz using an HS offset of 191 kHz with the frequency sweep direction determined by incrementing the phase as described by Eq. (3). However, when the direction of the sweep is reversed by replacing the cosh function with its reciprocal, the experimental enhancement was only about 2.8. Our explanation of this behavior is that to obtain maximum enhancement, the ssb from ST2 should be traversed first, followed by the ssb from ST1. SIMPSON simulations reproduce this behavior—if the ssb arising from ST1 is swept through first, then a lower enhancement is observed.

We were also curious to determine whether or not the DFS experiment is capable of providing signal enhancements by traversing only one set of ssbs and if the direction of the sweep is important. Experimentally it was found that the enhancements obtained for the ^{27}Al NMR CT of $Al(acac)_3$ was 2.5 regardless of whether the entire ssb manifold or one set of ssbs was swept. Further, it was found that, unlike for the case of the HS pulses, the enhancement obtained using DFS was relatively insensitive to the direction of the DFS sweep. These results suggest that under conditions of MAS, DFS behaves more like a saturation pulse, while HS pulses provide partial inversion of the satellite transitions.

Shown in Fig. 10 is a plot of the enhancements obtained from ^{27}Al NMR CT spectra versus HS offsets for a powder sample of $Al(acac)_3$, taken at 11.75 T spinning at 20 kHz. Increasing the offset from 40 to 160 kHz in steps of 20 kHz leads to a monotonic increase in the enhancement up to a maximum value of about 4.1. This plateau spans a frequency of about 100 kHz centered at approximately 200 kHz, the approximate frequency of the ST1 "horns" (see Fig. 10). At offsets greater than 260 kHz, the ST1 transitions no longer overlap with the ST2 transitions and similar to the spin-3/2 experiments, the enhancement starts to decrease with distortions appearing on the CT. Although the enhancement increases again as a function of HS offset (a second maximum occurs with an offset of 350 kHz), there are large distortions in the CT spectrum. For HS offset frequencies of between 550 and 780 kHz, the enhancement of the signal remains constant at approximately 1.4 to an offset of 800 kHz. As expected, no enhancement was observed for offsets beyond 800 kHz.

4.2.1.2. Effect of MAS frequency on the enhancement. The enhancement of the ^{27}Al NMR CT of $Al(acac)_3$ is dependent upon the spinning frequency of the sample with observed enhancements of 2.7, 3.3, 3.5, and 4.1 while spinning at 5, 10, 13, and 20 kHz, respectively. In each case the bw was set to ν_r. SIMPSON simulations reproduce this trend, which, so far, has been only observed for $Al(acac)_3$. The CT enhancement oscillated as a function of the ν_r with the HS offset when the offsets were incremented by 1 kHz steps. For example, while spinning at 5 kHz (bw = 5 kHz), maximum enhancements of about 2.7 occurred at HS offsets of 177, 182, 186, and 191 kHz (etc.) with minimum enhancements of about 2.5 with HS offsets of 179, 184, 189, and 194 kHz (etc.). Spinning at 10 kHz (bw = 10 kHz), maximum enhancements were observed for offsets of 172, 182, 192, and 202 kHz, with the maximum enhancement of 3.3 at 192 kHz and minimum enhancements of about 2.2 at offset values of 176, 186, 196, and 206 kHz. This behavior is illustrated in Fig. 11 and reproduced by SIMPSON. The reason for the oscillation in the enhancement with HS offset is consistent with the interpretation provided in the previous section; i.e., the ssbs from ST2 should be inverted first, followed by inversion of the ssb from ST1.

4.2.1.3. Effect of HS bandwidth on enhancement. The effect of HS bw on the enhancement of the ^{27}Al NMR CT from $Al(acac)_3$ spinning at 10 kHz was examined and analogous to the spin-3/2 case (Fig. 5), the maximum enhancement

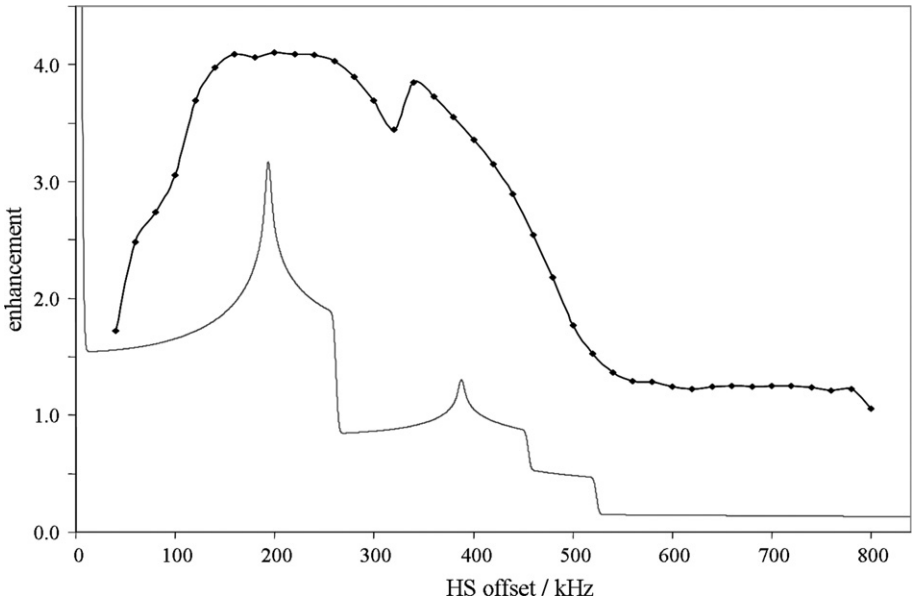

Fig. 10. Integrated intensity of the ^{27}Al NMR CT as a function of HS offset with bw of 20 kHz for a powder sample of Al(acac)$_3$ spinning at 20 kHz. $B_0 = 11.75$ T. Shown in the inset is one half of the calculated powder pattern for a stationary sample.

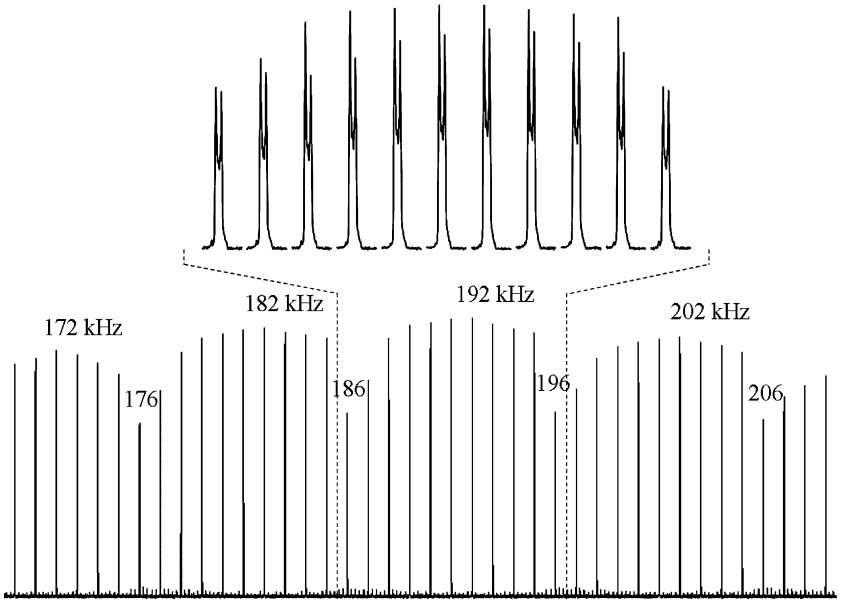

Fig. 11. A series of ^{27}Al CT NMR spectra of a powder sample of Al(acac)$_3$ spinning at 10 kHz as a function of the HS offset (bw = 10 kHz) in 1 kHz steps from 170 to 209 kHz.

was found when bw was equal to ν_r. The integrated area, normalized to 1.0 at maximum enhancement, versus bw is plotted in Fig. 12. To obtain the maximum enhancement with the least amount of distortion, the HS bw should be set to ν_r as found for the spin-3/2 case.

Distortions in some of the CT spectra due to HS pulses were also observed for the spin-5/2 case, particularly when the value of the HS offset was greater than approximately 300 kHz, even when the bw of the HS pulse is set to ν_r. Since the conduit for CT enhancement is through population transfer via the ssbs of the ST1, any asymmetry in the ssb due to unequal contributions from all crystallites will be transferred to the CT. Asymmetry in ST1 ssbs are well known [67].

4.2.1.4. Effect of HS rf-field and pulse duration on enhancement. As for spin-3/2 nuclei, the rf power level for the HS pulses should be above a certain threshold and the pulse width needs to be chosen properly in order to obtain an adiabatic HS pulse. Similar curves as the one shown in Fig. 8 are obtained for spin-5/2 nuclei. The rf field necessary for CT enhancement in the case of the spin-5/2 nuclei

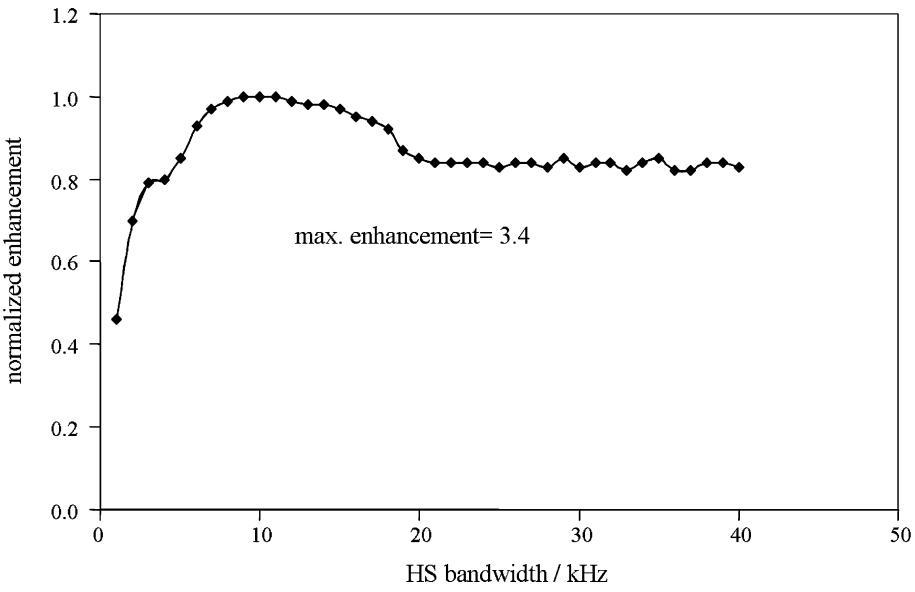

Fig. 12. Integrated intensity of the ^{27}Al NMR CT of Al(acac)$_3$ as a function of bw of the HS pulse with offset set to 190 kHz.

were found to be much lower than those used for spin-3/2 nuclei.

In conclusion, for our spin-5/2 test sample, Al(acac)$_3$, optimum enhancement with minimum distortion in the CT can be obtained when the HS bw is set to ν_r and the offset is in the vicinity of the "horns" associated with the ST1.

4.2.2. Further examples of spin-5/2 systems

The HS pulses were also applied to other spin-5/2 nuclei, ^{55}Mn and ^{127}I. The CT ^{55}Mn NMR spectra obtained from an MAS powder sample of $Mn_2(CO)_{10}$, $C_Q = 3.0$ MHz, and $\eta_Q = 0.5$ [68], were enhanced by 3.1 and 2.5 with HS and DFS [37], respectively. The smaller enhancement obtained here relative to the ^{27}Al case are attributed, as in the case of ^{23}Na NMR of Na_2MoO_4, to the very strong homonuclear dipolar coupling between the two neighboring ^{55}Mn, which is also responsible for the unusual shape for the CT [37]. The ^{127}I CT NMR spectra from an MAS powder sample of NH_4IO_4, $C_Q = 10.0$ MHz and $\eta_Q = 0.0$ [49], show an enhancement of 2.8 with HS versus 2.3 using DFS. In this case the smaller enhancements from ^{127}I are most likely due to the very short T_1 values of the STs which lead to significant population relaxation during the time of the HS pulse. Several other compounds containing spin-5/2 nuclei were also examined; the enhancements are summarized in Table 1. There is a reasonable spread in the enhancement values obtained for the spin-5/2 nuclei, ranging from 1.8 to 4.1. It is believed that rapid spin-lattice relaxation is at least partially responsible for the lower enhancements. For example, our kaolinite sample may contain small quantities of paramagnetic transition metal cations. It is interesting to note that SIMPSON simulations which do not include consideration of relaxation effects, predict a CT enhancement of 3.34 using an HS pulse positioned at an offset of 153 kHz from the CT. Furthermore, for kaolinite, the DFS experiment yielded an enhancement of 1.9 which is within experimental error of that obtained using the HS experiment.

Enhancements with HS on the CT NMR spectra of ^{27}Al and ^{55}Mn from stationary samples of Al(acac)$_3$ and $Mn_2(CO)_{10}$ [37] were also observed. As for spin-3/2 nuclei, HS gives slightly higher enhancements than DFS (4.0 for HS vs 3.8 for DFS in the case of Al(acac)$_3$ and for ^{55}Mn, enhancements of 3.2 vs. 3.0 were obtained with HS and DFS [37]).

5. Conclusions

A double or a single frequency HS pulse can be used to enhance the intensity of the central NMR transition of half-integer quadrupolar nuclei in MAS powder samples. These HS enhancement techniques generally provide higher factors than those obtained with other methods. For MAS powder samples of both spin-3/2 and spin-5/2 nuclei, the maximum enhancements are realized when the HS offsets are equal to the frequency corresponding to the maximum probability of crystallites within the sample, i.e., the position of the "horns" of ST1, and only one spinning sideband generated from the satellite transitions need be inverted for maximum enhancement. Thus, the bandwidth of the HS pulses should be set to the spinning frequency to ensure inversion of a complete ssb. A lower enhancement is found for spin-3/2 nuclei when the bandwidth is equal to twice the spinning speed and a smaller secondary maximum is found at three times the spinning speed. The duration of the HS pulse is not very critical provided it is above a threshold value. When applied to stationary powder samples, the enhancements realized using HS are comparable to those using DFS. Analogous with the DFS experiment, the HS must sweep as much of the satellite transition powder pattern as possible without saturating the CT.

Preliminary enhancement results for half-integer quadrupolar nuclei with $I > 3/2$ are very promising but will need further studies. The enhancement values obtained from spin-5/2 nuclei seem to be more variable than those found for spin-3/2 nuclei presumably because of shorter spin-lattice relaxation times. Central transition distortions can occur if only part of the ssb generated by ST1 is inverted by the HS pulse, as was found for the spin-3/2 case (see Fig. 7) or if only a small portion of the entire ensemble of crystallite orientations contribute to the inverted ssb, as found in the spin-5/2 case. The advantage of using the HS pulses over RAPT or DFS is in the potential higher enhancement values obtainable with HS. However, to obtain these higher values, HS experiments are harder to optimize for spin-5/2 systems because the enhancement varies with HS offset as a function of spinning frequency. For MAS samples, the DFS experiment is relatively easy to set up since one sweeps the entire powder pattern. Both RAPT, the new FSG-RAPT, and HS experiments require placing a pulse(s) at the proper location for optimum enhancement. That is, some estimate of the nuclear quadrupolar parameters is highly desirable for these experiments. On the other hand, knowledge of approximate nuclear quadrupolar coupling constants and asymmetry parameters is less important for the DFS experiments involving MAS samples. For stationary powder samples, prior knowledge of the quadrupolar parameters is equally important for the HS and DFS experiments. The use of repetitive-HS, as has been utilized with RAPT [23] and DFS [69], is also considered in order to realize even higher enhancements.

In summary, for NMR investigations of spin-3/2 and spin-5/2 nuclei, we highly recommend routine use of population transfer experiments utilizing HS pulses, particularly for low-γ nuclei such as ^{33}S, ^{53}Cr, ^{95}Mo, etc. Provided one does not sweep the HS pulse close to the central transition, such experiments can only lead to signal enhancement!

Acknowledgments

The authors wish to thank members of the solid-state NMR group at the University of Alberta for helpful comments and discussions about this work. In particular, we thank Kris Ooms for his help with some of the simulations as well as his interest in this project. We are grateful to Professor Christian Detellier and his co-workers at the University of Ottawa for kindly providing the sample of kaolinite. R.E.W. is a Canada Research Chair in Physical Chemistry at the University of Alberta and thanks the University of Alberta, the Natural Sciences and Engineering Research Council of Canada (NSERC) and the Government of Canada for research support.

References

[1] M.J. Duer (Ed.), Solid-State NMR Spectroscopy: Principles and Application, Blackwell Science, United Kingdom, 2002.

[2] D.L. Bryce, G.M. Bernard, M. Gee, M.D. Lumsden, K. Eichele, R.E. Wasylishen, Practical aspects of modern routine solid-state multinuclear magnetic resonance spectroscopy: one-dimensional experiments, Can. J. Anal. Sci. Spec. 46 (2001) 46–82.

[3] K.J.D. MacKenzie, M.E. Smith, Multinuclear Solid-State NMR of Inorganic Materials, Pergamon, Amsterdam, 2002.

[4] R.K. Harris, E.D. Becker, S.M. Cabral De Menezes, R. Goodfellow, P. Granger, NMR nomenclature. Nuclear spin properties and conventions for chemical shifts (IUPAC recommendations 2001), Pure Appl. Chem. 73 (2001) 1795–1818.

[5] A. Abragam, The Principles of Nuclear Magnetism, Oxford University Press, Oxford, 1961.

[6] R.V. Pound, Nuclear electric quadrupole interactions in crystals, Phys. Rev. 79 (1950) 685–702.

[7] Z. Gan, P. Srinivasan, J.R. Quine, S. Steuernagel, B. Knott, Third-order effect in solid-state NMR of quadrupolar nuclei, Chem. Phys. Lett. 367 (2003) 163–169.

[8] J.P. Amoureux, C. Fernandez, P. Granger, Interpretation of quadrupolar powder spectra: static and MAS experiments (tutorial session), in: P. Granger, R.K. Harris (Eds.), Multinuclear Magnetic Resonance in Liquids and Solids—Chemical Applications, Kluwer Academic Publishers, The Netherlands, 1990, pp. 409–424.

[9] S. Vega, Y. Naor, Triple quantum NMR on spin systems with $I = 3/2$ in solids, J. Chem. Phys. 75 (1981) 75–86.

[10] J. Haase, M.S. Conradi, Sensitivity enhancement for NMR of the central transition of quadrupolar nuclei, Chem. Phys. Lett. 209 (1993) 287–291.

[11] J. Haase, M.S. Conradi, C.P. Grey, A.J. Vega, Population transfers for NMR of quadrupolar spins in solids, J. Magn. Reson. A 109 (1994) 90–97.

[12] A.P.M. Kentgens, R. Verhagen, Advantages of double frequency sweeps in static, MAS and MQMAS NMR of spin $I = 3/2$ nuclei, Chem. Phys. Lett. 300 (1999) 435–443.

[13] P.K. Madhu, A. Goldbourt, L. Frydman, S. Vega, Sensitivity enhancement of the MQMAS NMR experiment by fast amplitude modulation of the pulses, Chem. Phys. Lett. 307 (1999) 41–47.

[14] Z. Yao, H.-T. Kwak, D. Sakellariou, L. Emsley, P.J. Grandinetti, Sensitivity enhancement of the central transition NMR signal of quadrupolar nuclei under magic-angle spinning, Chem. Phys. Lett. 327 (2000) 85–90.

[15] S. Prasad, H.T. Kwak, T. Clark, P.J. Grandinetti, A simple technique for determining nuclear quadrupole coupling constants with RAPT solid-state NMR spectroscopy, J. Am. Chem. Soc. 124 (2002) 4964–4965.

[16] T. Bräuniger, G. Hempel, P.K. Madhu, Fast amplitude-modulated pulse trains with frequency sweep (SW-FAM) in static NMR of half-integer spin quadrupolar nuclei, J. Magn. Reson. 181 (2006) 68–78.

[17] A.P.M. Kentgens, Quantitative excitation of half-integer quadrupolar nuclei by a frequency-stepped adiabatic half-passage, J. Magn. Reson. 95 (1991) 619–625.

[18] D. Iuga, H. Schäfer, R. Verhagen, A.P.M. Kentgens, Population and coherence transfer induced by double frequency sweeps in half-integer quadrupolar spin systems, J. Magn. Reson. 147 (2000) 192–209.

[19] H. Schäfer, D. Iuga, R. Verhagen, A.P.M. Kentgens, Population and coherence transfer in half-integer quadrupolar spin systems induced by simultaneous rapid passages of the satellite transitions: a static and spinning single crystal nuclear magnetic resonance study, J. Chem. Phys. 114 (2001) 3073–3091.

[20] D. Iuga, A.P.M. Kentgens, Influencing the satellite transitions of half-integer quadrupolar nuclei for the enhancement of magic angle spinning spectra, J. Magn. Reson. 158 (2002) 65–72.

[21] D. Iuga, Ph.D. thesis: Nuclear Magnetic Resonance Studies of Half-Integer Quadrupolar Nuclei: Sensitivity Enhancements using Double Frequency Sweep, Department of Chemistry, University of Nijmegen, 2003.

[22] H.-T. Kwak, S. Prasad, Z. Yao, P.J. Grandinetti, J.R. Sachleben, L. Emsley, Enhanced sensitivity in RIACT/MQ-MAS NMR experi-

ments using rotor assisted population transfer, J. Magn. Reson. 150 (2001) 71–80.
[23] H.T. Kwak, S. Prasad, T. Clark, P.J. Grandinetti, Enhancing sensitivity of quadrupolar nuclei in solid-state NMR with multiple rotor assisted population transfers, Solid State Nucl. Magn. Reson. 24 (2003) 71–77.
[24] H.T. Kwak, S. Prasad, T. Clark, P.J. Grandinetti, Selective suppression and excitation of solid-state NMR resonances based on quadrupole coupling constants, J. Magn. Reson. 160 (2003) 107–113.
[25] S.L. McCall, E.L. Hahn, Self-induced transparency, Phys. Rev. 183 (1969) 457–485.
[26] M.S. Silver, R.I. Joseph, C.N. Chen, V.J. Sank, D.I. Hoult, Selective-population inversion in NMR, Nature 310 (1984) 681–683.
[27] M.S. Silver, R.I. Joseph, D.I. Hoult, Highly selective pi/2 and pi-pulse generation, J. Magn. Reson. 59 (1984) 347–351.
[28] M.S. Silver, R.I. Joseph, D.I. Hoult, Selective pulse creation by inverse solution of the Bloch–Riccati equation, Magn. Reson. Med. 1 (1984) 294.
[29] M.S. Silver, R.I. Joseph, D.I. Hoult, Selective spin inversion in nuclear magnetic-resonance and coherent optics through an exact solution of the Bloch–Riccati equation, Phys. Rev. A 31 (1985) 2753–2755.
[30] J. Baum, R. Tycko, A. Pines, Broad-band and adiabatic inversion of a 2-level system by phase-modulated pulses, Phys. Rev. A 32 (1985) 3435–3447.
[31] Ē. Kupče, R. Freeman, Optimized adiabatic pulses for wideband spin inversion, J. Magn. Reson. A 118 (1996) 299–303.
[32] A. Tannűs, M. Garwood, Adiabatic pulses, NMR Biomed. 10 (1997) 423–434.
[33] M. Garwood, L. DelaBarre, The return of the frequency sweep: designing adiabatic pulses for contemporary NMR, J. Magn. Reson. 153 (2001) 155–177.
[34] D.G. Norris, Adiabatic radiofrequency pulse forms in biomedical nuclear magnetic resonance, Concepts Magn. Reson. 14 (2002) 89–101.
[35] Y.A. Tesiram, M.R. Bendall, Universal equations for linear adiabatic pulses and characterization of partial adiabaticity, J. Magn. Reson. 156 (2002) 26–40.
[36] R. Siegel, T.T. Nakashima, R.E. Wasylishen, Signal enhancement of NMR spectra of half-integer quadrupolar nuclei in solids using hyperbolic secant pulses, Chem. Phys. Lett. 388 (2004) 441–445.
[37] R. Siegel, T.T. Nakashima, R.E. Wasylishen, Sensitivity enhancement of solid-state NMR spectra of half-integer spin quadrupolar nuclei using hyperbolic secant pulses: applications to spin-5/2 nuclei, Chem. Phys. Lett. 421 (2006) 529–533.
[38] R. Siegel, T.T. Nakashima, R.E. Wasylishen, Sensitivity enhancement of MQMAS NMR spectra of spin 3/2 nuclei using hyperbolic secant pulses, Chem. Phys. Lett. 403 (2005) 353–358.
[39] R. Siegel, T.T. Nakashima, R.E. Wasylishen, Sensitivity enhancement of NMR spectra of half-integer quadrupolar nuclei in the solid state via population transfer, Concepts Magn. Reson. 26A (2005) 47–61.
[40] D. Freude, J. Haase, Quadrupole effects in solid-state nuclear magnetic resonance, in: P. Diehl, E. Fluck, H. Gunther, R. Kosfeld, J. Seelig (Eds.), NMR Basic Principles and Progress, Springer, Berlin, 1993, pp. 1–90.
[41] D. Freude, Quadrupolar nuclei in solid state nuclear magnetic resonance, in: R.A. Meyers (Ed.), Encyclopedia of Analytical Chemistry, John Wiley & Sons, Ltd, Tarzana, CA, USA, 2000, pp. 12188–12224.
[42] P.P. Man, Quadrupolar Interactions, in: D.M. Grant, R.K. Harris (Eds.), Encyclopedia of Nuclear Magnetic Resonance, John Wiley & Sons, Chichester, England, 1996, pp. 3838–3848.
[43] P.P. Man, Quadrupolar couplings in nuclear magnetic resonance, general, in: R.A. Meyers (Ed.), Encyclopedia of Analytical Chemistry, John Wiley & Sons, Ltd, Tarzana, CA, USA, 2000, pp. 12224–12265.
[44] A.J. Vega, Quadrupolar nuclei in solids, in: D.M. Grant, R.K. Harris (Eds.), Encyclopedia of Nuclear Magnetic Resonance, John Wiley & Sons, Chichester, England, 1996, pp. 3869–3889.
[45] M.R. Bendall, Heteronuclear *J*-coupling precession during spin-lock and adiabatic pulses. Use of adiabatic inversion pulses in high-resolution NMR, J. Magn. Reson. A 116 (1995) 46–58.
[46] E. Kupče, R. Freeman, Stretched adiabatic pulses for broadband spin inversion, J. Magn. Reson. A 117 (1995) 246–256.
[47] E. Van Veenendaal, B.H. Meier, A.P.M. Kentgens, Frequency stepped adiabatic passage excitation of half-integer quadrupolar spin systems, Mol. Phys. 93 (1998) 195–213.
[48] D. Rosenfeld, Y. Zur, Is the sech/tanh adiabatic pulse really adiabatic? J. Magn. Reson. 132 (1998) 102–108.
[49] G. Wu, S. Dong, High-field I-127 NMR of solid sheelite structures: periodates revisited, Solid State Nucl. Magn. Resn. 20 (2001) 100–107.
[50] M. Bak, J.T. Rasmussen, N.C. Nielsen, SIMPSON: a general simulation program for solid-state NMR spectroscopy, J. Magn. Reson. 147 (2000) 296–330.
[51] J. Skibsted, H.J. Jakobsen, Variable-temperature Rb-87 magic-angle spinning NMR spectroscopy of inorganic rubidium salts, J. Phys. Chem. A 103 (1999) 7958–7971.
[52] F.H. Larsen, H.J. Jakobsen, P.D. Ellis, N.C. Nielsen, Sensitivity-enhanced quadrupolar-echo NMR of half-integer quadrupolar nuclei. Magnitudes and relative orientation of chemical shielding and quadrupolar coupling tensors, J. Phys. Chem. A 101 (1997) 8597–8606.
[53] E.L. Hahn, Spin echoes, Phys. Rev. 80 (1950) 580–594.
[54] R. Siegel, T.T. Nakashima, R.E. Wasylishen, Signal-to-noise enhancement of NMR spectra of solids using multiple-pulse spin-echo experiments, Concepts Magn. Reson. 26A (2005) 62–77.
[55] H.Y. Carr, E.M. Purcell, Effects of diffusion on free precession in nuclear magnetic resonance experiments, Phys. Rev. 94 (1954) 630–638.
[56] S. Meiboom, D. Gill, Modified spin-echo method for measuring nuclear relaxation times, Rev. Sci. Instrum. 29 (1958) 688–691.
[57] F.H. Larsen, H.J. Jakobsen, P.D. Ellis, N.C. Nielsen, QCPMG-MAS NMR of half-integer quadrupolar nuclei, J. Magn. Reson. 131 (1998) 144–147.
[58] M. Mehring, Principles of High Resolution NMR in Solids, Springer, Berlin, Heidelberg, New York, 1983.
[59] K. Schmidt-Rohr, H.W. Spiess, Multidimensional Solid-State NMR and Polymers, Academic Press, London, 1999.
[60] M. Mehring, V.A. Weberruss, Object-Oriented Magnetic Resonance: Classes and Objects, Calculations and Computations, Academic Press, London, UK, 2001.
[61] S.E. Ashbrook, S. Wimperis, Rotor-synchronized acquisition of quadrupolar satellite-transition NMR spectra: practical aspects and double-quantum filtration, J. Magn. Reson. 177 (2005) 44–55.
[62] A. Samoson, Satellite transition high-resolution NMR of quadrupolar nuclei in powders, Chem. Phys. Lett. 119 (1985) 29–32.
[63] P. Caravatti, G. Bodenhausen, R.R. Ernst, Selective pulse experiments in high-resolution solid state NMR, J. Magn. Reson. 55 (1983) 88–103.
[64] J. Skibsted, H.J. Jakobsen, ^{23}Na Magic-angle spinning nuclear magnetic resonance of central and satellite transitions in the characterization of the anhydrous, dihydrate, and mixed phases of sodium molybdate and tungstate, Solid State Nucl. Magn. Resn. 3 (1994) 29–38.
[65] M.A.M. Forgeron, R.E. Wasylishen, unpublished results.
[66] R.W. Schurko, R.E. Wasylishen, H. Foerster, Characterization of anisotropic aluminum magnetic shielding tensors. Distorted octahedral complexes and linear molecules, J. Phys. Chem. A 102 (1998) 9750–9760.
[67] J. Skibsted, N.C. Nielsen, H. Bildsøe, H.J. Jakobsen, Satellite transitions in MAS NMR spectra of quadrupolar nuclei, J. Magn. Reson. 95 (1991) 88–117.
[68] S. Wi, L. Frydman, Residual dipolar couplings between quadrupolar nuclei in high resolution solid state NMR: description and observations in the high-field limit, J. Chem. Phys. 112 (2000) 3248–3261.

[69] A.P.M. Kentgens, E.R.H. van Eck, T.G. Ajithkumar, T. Anupold, J. Past, A. Reinhold, A. Samoson, New opportunities for double rotation NMR of half-integer quadrupolar nuclei, J. Magn. Reson. 178 (2006) 212–219.

[70] G. Engelhardt, H. Koller, A simple procedure for the determination of the quadrupole interaction parameters and isotropic chemical-shifts from magic angle spinning NMR-spectra of half-integer spin nuclei in solids, Magn. Reson. Chem. 29 (1991) 941–945.

[71] B. Filsinger, P. Gutsche, U. Haeberlen, N. Weiden, Search for a magnetic-field dependence of the interaction of the nuclear quadrupole moment with the electric-field gradient, J. Magn. Reson. 125 (1997) 280–290.

[72] G.S. Crosson, S. Choi, J. Chorover, M.K. Amistadi, P.A. O'Day, K.T. Mueller, Solid-state NMR identification and quantification of newly formed aluminosilicate phases in weathered kaolinite systems, J. Phys. Chem. B 110 (2006) 723–732.

[73] Y.V. Shulepov, A.S. Litovchenko, A.A. Melnikov, V.Y. Proshko, V.V. Kulik, The effects of quadrupole splitting of the central ^{27}Al NMR line in polycrystalline kaolinite, J. Magn. Reson. 53 (1983) 178–186.